Highly Accurate Grey Neural Network Classifier for an Abdominal Aortic Aneurysm Classification Based on Image Processing Approach

Anandh Sam Chandra Bose
Department of Biomedical Engineering, Saveetha
Engineering College, India
anandhbose123@gmail.com

Vasuki Ramesh
Department of Biomedical Engineering, Bharath Institute of
Higher Education and Research, India
hod.bme@bharathuniv.ac.in

Abstract: *An Abdominal Aorta Aneurysm (AAA) is an abnormal focal dilation of the aorta. Most un-ruptured AAAs are asymptomatic, which leads to the problem of having abdominal malignancy, kidney damage, heart attack and even death. As it is ominous, it requires an astute scrutinizing approach. The significance of this proposed work is to scrutinize the exact location of the ruptured region and to make astute report of the pathological condition of AAA by computing the Ruptured Potential Index (RPI). To determine these two factors, image processing is performed in the retrieved image of aneurysm. Initially, it undergoes a process to obtain a high-quality image by making use of Adaptive median filter. After retrieving high quality image, segmentation is carried out using Artificial Neural Network-based segmentation. After segmenting the image into samples, 12 features are extracted from the segmented image by Gray Level Co-Occurrence Matrix (GLCM), which assists in extracting the best feature out of it. This optimization is performed by using Particle Swarm Optimization (PSO). Finally, Grey Neural Network (GNN) classifier is applied to analogize the trained and test set data. This classifier helps to achieve the targeted objective with high accuracy.*

Keywords: *Adaptive median filter, artificial neural network-based segmentation, GLCM, PSO, gray neural network classifier.*

1. Introduction

The Abdominal Aorta Aneurysm (AAA) is a permanent localized dilation of the abdominal aorta. When the aneurysm begins to expand, the exalted wall tension causes the problem of rupture. The factors like atherosclerosis, smoking and genetics are the significant causes of AAA. The prospective studies have suggested that the AAA has to be given proper treatment when the diameter exceeds above 0.8 cm and over the period of 6 months, if the growth rate exceeds 0.8 cm. There arises a major risk. Based upon the aneurismal size and rate of growth, the risk of rupture is analyzed. It is thus highly mandatory to provide proper medication or treatment as soon as possible to minimize the mortality rate. The existence of thrombus, calcification and vessel tortuosity are the main factors involved in AAA. The astute screening is highly essential for improving the AAA surgical procedures. The existing approaches have used some techniques based on the Fluid Structure Interaction (FSI) simulation of AAA, pulse wave imaging and Computational Solid Stress (CSS) prediction [1, 2, 7, 19, 22, 27]. When analogizing with CSS prediction, FSI is given highest preference. Though it generates beneficial result, it creates a complex mesh for an already complicated domain. In addition, it is computationally expensive.

In this proposed work, the image processing is performed to get an astute result. Initially, an aneurysm image is processed in the preprocessing stage with the aid of an adaptive median filter. It is a facile smoothing filter, which helps to gain an enhanced image. After this process, it undergoes a process of splitting the enhanced image into samples [13, 17, 18]. The extraction of 12 features is done by using GLCM technique [9, 12, 14, 15, 16]. Particle Swarm Optimization is employed to pick out the best feature in consideration with a given measure of quality [23, 25, 26]. Finally, the classifier helps to perform comparative analysis between the trained and test set data. The existing approaches using the Support Vector Machine (SVM) classifier, fuzzy logic and Artificial Neural Network (ANN) fail to deliver optimal outcomes [3, 6, 8, 10, 11, 21]. Even though the fuzzy is quite good in handling uncertainties, it is fully dependent on human expertise and so it takes more time to perform computation [4, 5, 20, 24]. In this study, the GNN classifier is used to get rid of this issue and to minimize the time consumption. It has a good capacity to easily recognize the nonlinear relationship. The detailed description of this technique is explained in the upcoming section.

2. Related Works

Auricchio *et al*. [2] have proposed a regression technique to analyze the aorta aneurysmal tissue. The response surfaces of ultimate stretch, stress and coefficients in patient data function, which have been obtained from the clinical practice are built by using the regression model proposed in this paper. However, the investigation concerning the dynamics of aneurysm rupture is highly complicated.

Apostolakis *et al*. [1] have proposed a pulse wave imaging technique for automatic inhomogeneity detection of spatial vessel. To diagnose the arterial problems in an easier way, an adaptive Pulse Wave Imaging (PWI) technique has been employed and its properties are tested. Based on the diameter waveform, it initiates the error between the adaptive PWI interfaces. Do *et al*. [7] have proposed a Gaussian process for predicting the aneurysm growth with the assistance of Computed Tomography (CT) scans. By using the spatio-temporal field in the trained data, the concealed region from the point cloud data are evaluated. The forecast made through this process results in uncertainty because forecasting the 3D shape of aneurysmal growth is made in this study for the first time. Polanczyk *et al*. [19] have introduced a method to reconstruct the pulsatile hemodynamic in AAA by using patient-specific human cardiovascular system. Under different hemodynamic conditions, the hemodynamic changes are done with the help of the Human Cardiovascular System Phantom (HCSP). The analyzed vessel is supplied by the specified amount of medium in each time. The complications like stent-graft's migration, angular bands and Endoleaks have occurred in Endovascular Aneurysm Repair (EVAR) method.

Ren *et al*. [22] have implemented a 3D reconstruction of AAA based on iterative optimization. To improve the blurriness of outer contour and to increase the quality and the projection of the image, an efficient method has been employed. The accuracy of the abdominal aortic aneurysm reconstruction with the high stability, feasibility and speed has been attained. When the aneurysm wall experiences any depression, the possibility of the AAA rupture becomes high.

3. Proposed Work

The significant goal of this proposed work is to detect the exact location of the defected region and the pathological condition of AAA by evaluating the Ruptured Potential Index (RPI). The initial operation of this proposed work indicated in Figure 1 is regarded as preprocessing, which is carried out by the implementation of Adaptive median filter. It assists in not only eliminating the noises in the image but also in preserving the very fine details for delivering the output with maximum accuracy. After obtaining the standard image, it is split into multiple samples through the pixel-wise processing, which has a capability of extracting the nonlinear complicated relation between the dependent and non-dependent variables. After the segmentation process, a number of texture features are obtained by using the Gray Level Co-Occurrence Matrix (GLCM). In different aspects, it helps to gain the total average of correlation between the pair of pixels. The retrieved feature is optimized through the implementation of Particle Swarm Optimization (PSO) to get the best feature out of the obtained features. The last step is to perform comparative analysis between the trained and test set data. Both the grey system model and neural network combined classifier are utilized to enhance the performance of the system. It is feasible and effective for the time series prediction. It has a facile computing process and it generates an astute result. The working mechanisms and modelling of the entire system are elaborately described in the subsequent section.
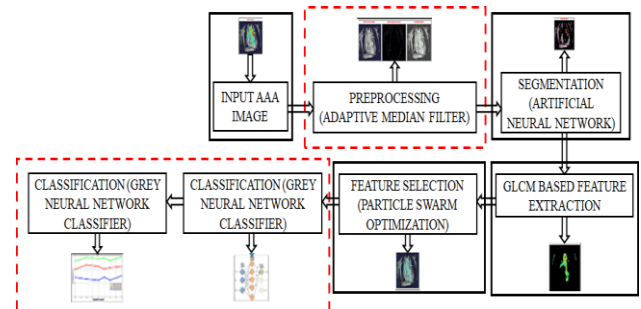
Figure 1. Block diagram of proposed work.

3.1. Adaptive Median Filter

During the process of image acquisition and transmission, the noisy distortion is always occurred. It represents that the pixel of image has varied intensity, which limits the objective of obtaining an accurate pixel value. The primary objective of this adaptive median filter is to filter the noises in the image of aneurysm in a manner that the real image is perceptible. It helps to eliminate the noises in the image and generates high performance. The Adaptive median filter is designed on the basis of two significant statistical measures like mean and variance. Moreover, the computational time is equal to the time to corrupt the degree of image corruption. It has a good capability to handle the impulsive noises. The operation modes of this filter are significantly demonstrated in the following passage.

Mode 1 determines whether the result of adaptive median filter is an impulse or not. If it is not impulsive, move on to mode 2. If it found to be impulsive, the size of the window is maximized. It attains Z_{med} when it is not an impulsive.
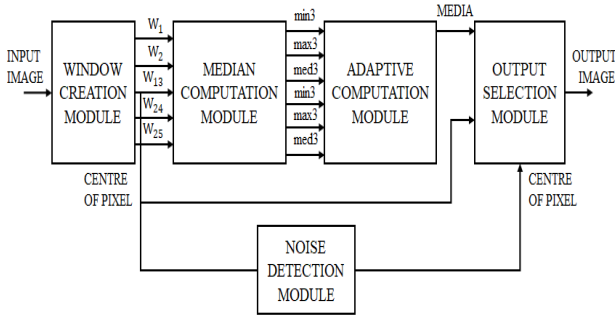
Figure 2. Adaptive median filter representation.

Mode 2 determines whether Zxy an impulse is or not. If it found to be non-impulsive, it results in the fixed pixel value Zxy. If it is impulsive, the algorithm returns to Z med. Figure 2 depicts the overall representation of Adaptive median filter and Figure 3 depicts the flowchart of adaptive median filter.
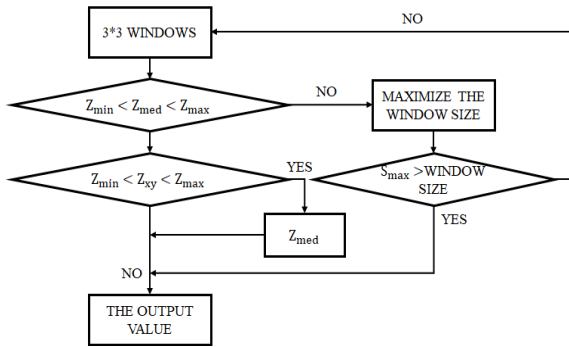
Figure 3. Flowchart of adaptive median filter.

3.2. Artificial Neural Network Based Segmentation

The segmentation of aneurysm plays a prominent role because an erroneous representation of segmentation affects the accuracy of feature extraction and determination on the basis of the segmented defected region. It involves the process of splitting the image into meaningful segments and this work involves ANN for segmentation as shown in Figure 4. It is the process by which the computation transforms an array of gray levels into segments with uniform and homogeneous characteristics. Initially, the gradient values of all the pixel in the image are evaluated and then the local maxima pixels are retrieved. The next process is to choose an extrema among all the extrema with the higher gradient norm. The value of the norm has to be higher than the maximized threshold.
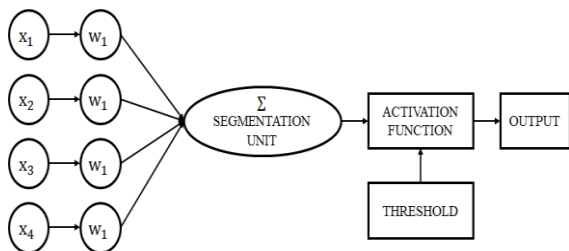
Figure 4. Artificial neural network-based segmentation.

N inputs are taken and consociated weights are specified as W_N. The segmentation is described as partitioning the image I into X_1, X_2,…, X_n. The computation is performed as follows,

$$I = \bigcup_{i=1}^{n} x_i \tag{1}$$

$$x_i \cap_{i \neq j} x_j = \emptyset \tag{2}$$

The input vector, $X_i = x_1, x_2, x_3, …, x_n$ is applied to the input unit and the output vector o_i is the observed output. Weight w_{ij} is computed as,

$$\Delta_i w_n j = \beta \delta_{ij} O_{ij} \tag{3}$$

$$\delta_{ij} = \begin{cases} f(net_{ij})\Sigma_k \delta_{ik} w_{kj} \ for \ a \ hidden \ node \\ (x_{ij} - O_{ij})f'(net \ ij) for \ an \ output \ node \end{cases}$$

Here, $net_{ij} = \Sigma_k w_{kj} O_{jk} + \theta_j$ acts as the overall input to node j by taking θ_j as a bias term $\emptyset$. The activation function is evaluated as,

$$F(x) = \frac{1}{1 + exp^{-1}} \tag{4}$$

3.3. Feature Extraction Using GLCM

The Gray level co-occurrence matrix is a method to retrieve the statistical features of defected region of AAA from the partitioned image. It is regarded as a crucial step because the result of this technique helps in the process of pattern recognition. It classifies the defected image to clearly recognize the erroneous information in the image of aneurysm. The GLCM is represented in a matrix format. By the matrix element $p(r, k)|\Delta_x, \Delta_y)$, two pixels are dissociated with the distance of pixel (Δ_x, Δ_y).

Given M× N neighborhood of aneurysm input image includes grey level with the range of 0 to G-1.

$$P(r, k|\Delta_x, \Delta_y) = WQ(r, k)|\Delta_x, \Delta_y) \tag{5}$$

Where, $$W = \frac{1}{(M - \Delta_x)(N - \Delta_y)} \tag{6}$$

$$Q(r, k|\Delta_x, \Delta_y) = \Sigma_{n=1}^{\Delta - \Delta y} \Sigma_{m=1}^{M - \Delta x} A \tag{7}$$

$$A = \begin{cases} 1 \ if \ (m,n) = r \ and \ f(m + \Delta x, n + \Delta y) = k \\ 0, \qquad elsewhere \end{cases} \tag{8}$$

Here, μ represent the mean value. Consider μ_x, μ_y, σ_x, σ_y as mean and standard deviation of p_x and p_y It is computed as,

$$p_x(r) = \Sigma_{k=0}^{G-1} p(r, k) \tag{9}$$

$$p_y(k) = \Sigma_{r=0}^{G-1} p(r, k) \tag{10}$$

$$\mu_x = \Sigma_{r=0}^{G-1} i \Sigma_{k=0}^{G-1} p(r, k) = \Sigma_{r=0}^{G-1} r p_x(r) \tag{11}$$

$$\mu_y = \Sigma_{r=0}^{G-1} \Sigma_{k=0}^{G-1} k(p(r, k) = \Sigma_{k=0}^{G-1} k p_y(k) \tag{12}$$

$$\sigma_x^2 = \Sigma_{r=0}^{G-1}(r - \mu_x)^2 \Sigma_{k=0}^{G-1} p(r, k) = \Sigma_{r=0}^{G-1}(p_x(r) - \mu_x(r))^2 \tag{13}$$

$$\sigma_y^2 = \Sigma_{k=0}^{G-1}(k - \mu_y)^2 \Sigma_{r=0}^{G-1} P(r, k) = \Sigma_{k=0}^{G-1}(P_Y(k) - \mu_y(k))^2 \tag{14}$$

$$P_{x+y}(k) = \Sigma_{i=0}^{G-1} \Sigma_{j=0}^{G-1} p(r, k) \quad r + k = c \tag{15}$$
$$For \ c = 0, 1, …, 2(G - 1)$$

$$P_{x-y}(c) = \Sigma_{r=0}^{G-1} \Sigma_{k=0}^{G-1} P(r, k) \quad |r - k| = c \tag{16}$$

The following 12 features are used in this work.

- Homogeneity: it involves only a small amount of gray levels by giving GLCM a corresponding maximum value of p (r, k). Hence, the generated sum of squares is large.

$$Homogeneity = \sum_{r=0}^{G-1} \sum_{k=0}^{G-1} \{P(r,k)\}^2 \qquad (17)$$

- Contrast: it is determined by the variation in the color and brightness of the image. The contrast is computed as,

$$Contrast = \sum_{n=0}^{G-1} n^2 \{\sum_{r=1}^{G} \sum_{k=1}^{G} p(r,k)\}, |r-k| = n \qquad (18)$$

- Inverse Difference Moment (IDM): the weighting factor $(1 + (r - k)^2)^{-1}$ inverse difference moment obtains less contribution from different dimensional space $(i \neq j)$. The obtained value of IDM is low in different dimensional space and high for uniform dimension.

$$IDM = \sum_{r=0}^{G-1} \sum_{k=0}^{G-1} \frac{1}{1+(r-k)^2} p(r,k) \qquad (19)$$

- Entropy: the non-uniform space has a first order entropy and a uniform space has a maximum entropy.

$$Entropy = -\sum_{r=0}^{G-1} \sum_{k=0}^{G-1} P(r,k) \times \log(P(r,k)) \qquad (20)$$

- Correlation: it calculates the gray level linear dependence between the pixels at certain position correspond to each other.

$$Correlation = \sum_{r=0}^{G-1} \sum_{k=0}^{G-1} \frac{\{r \times k\} \times P(r,k) - \{\mu_x \times \mu_y\}}{\sigma_x \times \sigma_y} \qquad (21)$$

- Variance: the value, which vary from the average value of $P(i,j)$ has relatively maximum weight. It is evaluated as,

$$variance = \sum_{r=0}^{G-1} \sum_{k=0}^{G-1} (r-\mu)^2 P(r,k) \qquad (22)$$

- Sum average:

$$Average = \sum_{r=0}^{2G-2} r P_{x+y}(r) \qquad (23)$$

- Overall Entropy:

$$Sum\ entropy = -\sum_{r=0}^{2G-2} P_{x+y}(r) \log(P_{x+y}(r)) \qquad (24)$$

- Difference Entropy:

$$Difference\ entropy\ -\sum_{r=0}^{G-1} P_{x+y}(r) \log(P_{x+y}(r)) \qquad (25)$$

- Inertia:

$$Inertia = \sum_{r=0}^{G-1} \sum_{k=0}^{G-1} \{r-k\}^2 \times P(r,k) \qquad (26)$$

- Cluster shade: the main contribution of this feature is to minimize the number of operations by determining the texture feature in the form of image pixel.

$$Cluster\ shade = \sum_{r=0}^{G-1} \sum_{k=0}^{G-1} \{r+k-\mu_x-\mu_y\}^3 \times P(r,k) \qquad (27)$$

- Cluster prominence: it is the simplest form of cluster shade. The cluster prominence is computed as,

$$Cluster\ prominence = \sum_{r=0}^{G-1} \sum_{k=0}^{G-1} \{r+k-\mu_x-\mu_y\}^4 \times P(r,k) \qquad (28)$$

These 12 extracted features help to get the exact location of defected region of AAA.

3.4. Particle Swarm Optimization

It plays a prominent role in recognizing the exact location of defected region. It is the mathematical computation in identifying the maxima and minima of functions. Here, the objective and constraint function are non-differentiable. In PSO, the current position is initially evaluated, which is then analogized with previous best and neighborhood best to identify the best solution. Two major roles in particle swarm optimization are exploitation and exploration. In exploitation, preferring the best solution is performed and in exploration, it searches the optimal solution. Its main aim is to minimize the function. A maximization function is converted to a minimization function as,

$$\max f(x) = \min f(x) \qquad (29)$$

In N dimensional space, each particle is considered as a point. Each particle has a position and velocity consociated with it. The particle agitate to alter its position on the basis of the position and velocities of current. Each particle memorizes the best identified location and the particles communicate the information of the best location, which are explored. Initially, the position and velocity are produced randomly with search space. The particle velocity is determined as,

$$V_i = wv_i + c_1 r_1 (p_{best} - X_i) + c_2 r_2 (g_{best} - X_i) \qquad (30)$$

Where C_1 and C_2 are acceleration coefficients, r_1 and r_2 are random number between o to 1.

Position of a particle is modified as,

$$X_i = X_i + v_i \qquad (31)$$

Then evaluate the objective function f_i and update the population, irrespective of the fitness. Update P_{best} and g_{best} if $f_i < f_{best,i}$.

$$P_{best,i} = x_i \qquad (32)$$

$$f_{best,i} = f_i \qquad (33)$$

If $f_{p_{best,i}} < f_{g_{best}}$

$$g_{best} = p_{best,i} \qquad (34)$$

$$f_{best} = f_{p_{best,i}} \qquad (35)$$

- Working of particle swarm optimization:

$$Consider\ \min f(x) = \sum_{i=1}^{4} x_i^2;\ \ 0 \leq x_i \leq 10 \qquad (36)$$

- Decision variables: $x_1, x_2, x_3,$ and x_4

  - Stage 1: Fix the size of population and maximum iteration.
  - Stage 2: Determine the random position and compute the fitness.
  - Stage 3: Produce random velocities within the domain of the variable.
  - Stage 4: Finally, identify the personal and global best of all solution.

3.5. Grey Neural Network Classifier

A coupled model of grey model and neural network is presented to predict the defected region of AAA and the pathological condition. It has an advantage of fast solving speed and it helps to express the nonlinear relationship in an easy manner. The Grey Neural Network (GNN) classifier shown in Figure 5 has a good capability of astutely predicting the large sample of data.

In certain precision, the neural network uses certain values but it gets fluctuated in case of any error. Consider f(x). Here x is to indicate the estimated result. The result of neural network is attained as a grey number. The Grey model is used to process the region with clear grey characteristics and neural network is to process the region without grey characteristic. Both have indirect connection with each other.
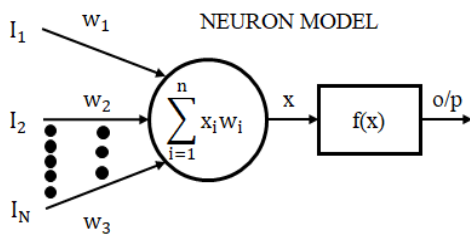
Figure 5. GNN classifier representation diagram.

- Modeling mechanism of Grey neural network classifier

The real data sequence is represented as,

$$x^{(0)}(t), t = 1,2, \dots, n \tag{37}$$

Accumulated generation of real data is evaluated as,

$$x^{(1)}(t) = \sum_{i=1}^{t} x^{(0)}(i), t = 1,2, \dots, n \tag{38}$$

The grey model is represented as follows,

$$\frac{d^2 x^{(1)}(t)}{dt^2} + a \frac{dx^{(1)}(t)}{dt} = b \tag{39}$$

Solve a and u by means of least square

$$[\hat{a}, \hat{b}] = \emptyset = (B^t B)^{-1} B^T y \tag{40}$$

$$\text{Where B=} \begin{bmatrix} -x^{(0)}(2)1 \\ -x^{(0)}(3) \ 1 \\ . \\ . \\ -x^{(0)}(n) \ 1 \end{bmatrix} \tag{41}$$

$$\text{Y=} \begin{bmatrix} x^{(0)}(2) - x^{(0)}(1) \\ x^{(0)}(3) - x^{(0)}(2) \\ . \\ . \\ x^{(0)}(n) - x^{(0)}(n-1) \end{bmatrix} \tag{42}$$

By solving Equation (37), the time response function is obtained as,

$$\hat{x}^{(1)}(k+1) = \left[\frac{b}{a^2} - \frac{x^{(0)}(1)}{a}\right] e^{-ak} + \frac{b}{a}(k+1) + [x^{(0)}(1) - \frac{b}{a}]\frac{(1+a)}{a} \tag{43}$$

To find out the parameter 'a' and 'b', the subsequent steps are followed.

- *Step* 1: Initially, the equation is mapped by the GNN.
- *Step* 2: The network is trained and the performance is satisfactory.
- *Step* 3: From the trained network, related weights are taken.
- *Step* 4: Finally, parameter a, b and u are evaluated. Thus, it generates an astute report.

4. Result and Discussion

The proposed work focuses on the identification of exact location of defected region and on the diagnosis of the pathological condition. It is elaborately discussed in this paper and the entire work is validated in MATLAB. The specimens of 100 samples are taken for performing the accurate analysis of AAA.

a) Input image 1.   b) Input image 2.
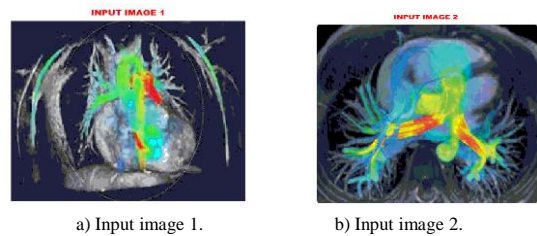
Figure 6. Input image of aneurysm.

Initially, the input image shown in Figure 6 is retrieved and it undergoes a process of filtering. The filter generates the image without any distortion and produces high quality image. The Adaptive median filter works well in handling high impulsive noise and the time taken is equal to the degree of corrupted image of aneurysm being filtered.

a) Grey scale image. b) Noise reduced data. c) Filtered image.

c) Grey scale image. d) Noise reduced data. e) Filtered image.
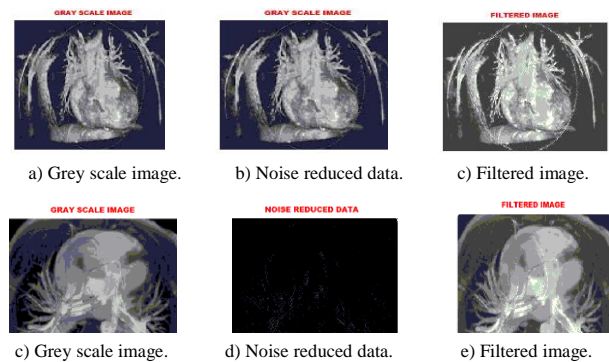
Figure 7. Filtered result of gray scale image.

Figure 7 shows the noise reduced filtered image. The input image is processed by using adaptive median filter. After obtaining the gray scale image, the noise is reduced and the filtered image is further processed in an enhanced manner as given in Figure 8. The generated binary pattern helps in the process of classification. While performing computation in binary pattern, the uniform patterns are used because of having a separate label and all the non uniform patterns are considered as a single label. Figure 9 shows the processed binary pattern of the image.

a) Binary image 1.   b) Enhanced image 1.

c) Binary image 2.   d) Enhanced image 2.
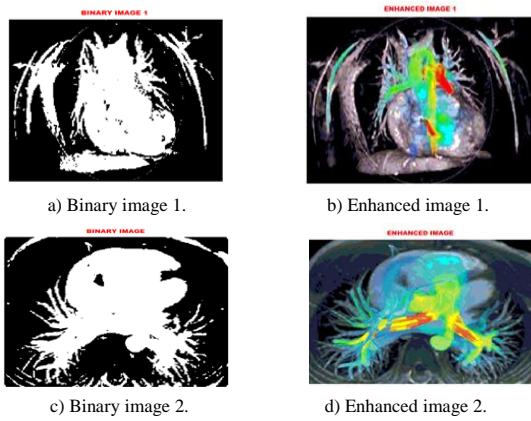
Figure 8. Enhanced image.

a) Pattern 1.   b) Pattern 2.
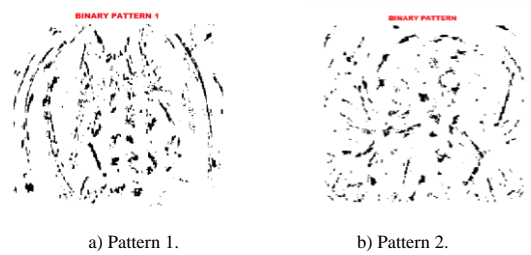
Figure 9. Binary pattern.

a) Image 1.   b) Image 2.
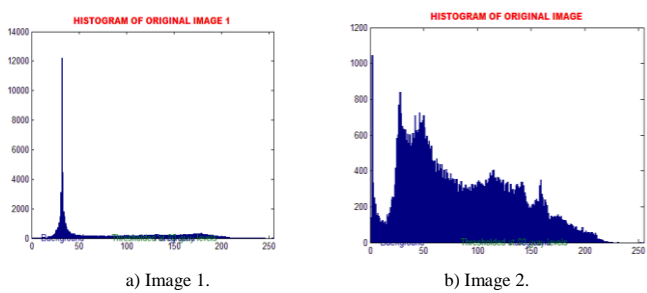
Figure 10. Histogram of original image.

Figure 10 represents the histogram of original image. The value of threshold ranges from 0 to 255. The histogram helps in graphically summarizing the distribution of a differentiated dataset. It shows the midpoint of the image, outlier and skewness to process the image in an efficient way.

a) Image 1.   b) Image 2.   c) Image 3.

d) Image 4.   e) Image 5.   f) Image 6.
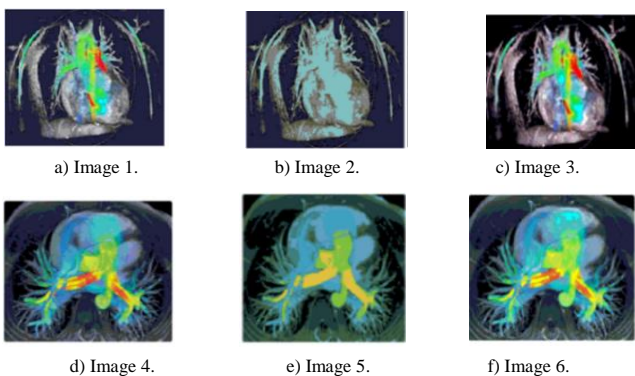
Figure 11. Grouping of images.

After the filtering process, the image grouping is performed and it shown in Figure 11. While performing grouping operation, the features which belong to a same group are extracted and an intermediate representation is retrieved to describe the key image of aneurysm.

a) Cluster 1.   b) Cluster 2.   c) Cluster 3.

d) Cluster 1.   e) Cluster 2.   f) Cluster 3.
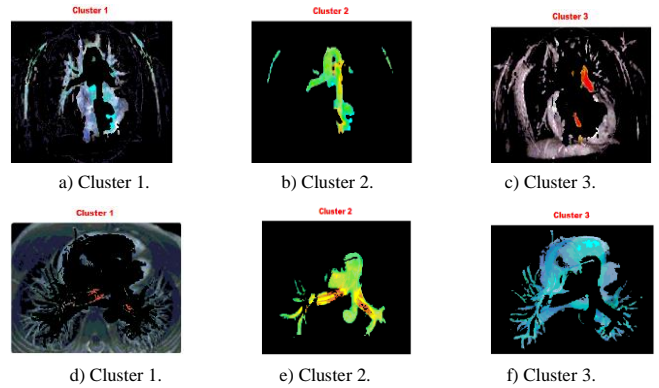
Figure 12. Clustered image.

a) Image 1.   b) Image 2.
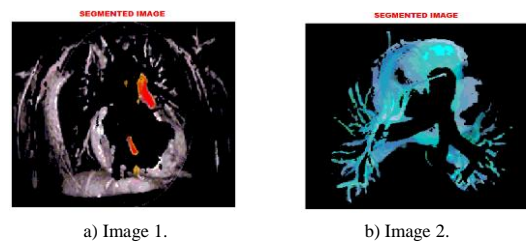
Figure 13. Segmented image.

The image of aneurysm is segmented into 256 samples. It involves a technique of transforming the obtained enhanced image into region of pixels. By performing this segmentation operation as indicated in Figures 12 and 13, optimal outcome is obtained since it process only the significant segments of the image instead of processing the entire image.

- Performance parameter: the performance parameters are analyzed by comparing the proposed work with another existing approaches. For multiple input samples, the proposed work shows the high performance by achieving the accuracy of 99.2% as given in Figure 14.
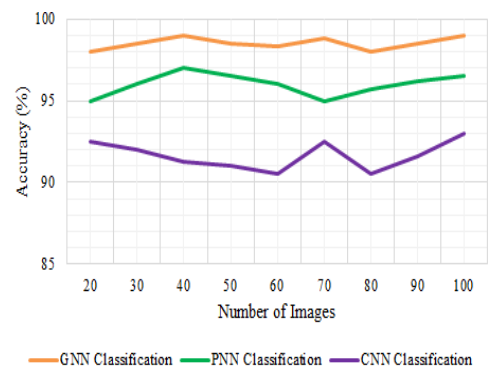
Figure 14. Accuracy comparison.

When analogizing with other two classifiers, the Gray neural network classifier shows high specificity of 99.1%, which is remarkably portrayed in the Figure 15. The specificity of proposed work is maintained constantly for multiple images.
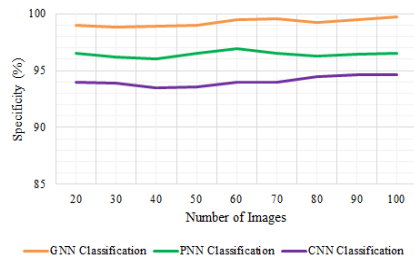
Figure 15. Specificity comparison.

Figure 16. Sensitivity comparison.

Figure 16 graph shows the sensitivity comparison between three classifiers. The proposed classifier reaches sensitivity of 99%. Even though there is a slight decrease in the value, it is constantly maintained after the number of images exceeds above 80. Table 1 indicates the comparison of F-score and evaluation time while Table 2 denotes the comparison of astuteness and precision.

Table 1. Comparison table of F-Score and evaluation time.

Input No.	F - Score		Evaluation time (ns)	
	Without PSO	With PSO	Without PSO	With PSO
Input 1	89.1	99.6	0.91	0.85
Input 2	87.56	98.2	0.90	0.88
Input 3	89.34	99.2	0.93	0.86
Input 4	87.33	97.6	0.912	0.83
Input 5	88.32	98.23	0.96	0.89
Input 6	89.9	99.35	0.92	0.82
Input 7	87.65	98.75	0.925	0.79
Input 8	86.43	97.9	0.93	0.75
Input 9	88.5	99.5	0.95	0.84
Input 10	88.92	98.82	0.87	0.933

Table 2. Comparison table of astuteness and precision.

Input No	Astuteness		Precision	
	Without PSO	With PSO	Without PSO	With PSO
Input 1	89.6	98	88.32	97.6
Input 2	88.3	98.4	87.43	97.53
Input 3	89.4	98.6	88.23	98.9
Input 4	87.9	97.9	89.3	97.1
Input 5	89.1	98.23	89.67	98.78
Input 6	88.65	97.93	87.65	98.05
Input 7	87.33	97.43	88.23	97.55
Input 8	89.45	98.42	88.9	97.42
Input 9	89	96.9	89.92	98
Input 10	87.5	98.95	87.9	98.75

In order to validate the introduced PSO approach, it is analogized with the existing topologies like Genetic Algorithm (GA) and Differential Evolution (DE) in relevance to the parameters like astuteness and evaluation time, which proves that the proposed PSO

delivers optimum outcomes than the other approaches as highlighted in Figure 17.

a) Evaluation time comparison.

b) Astuteness comparison.
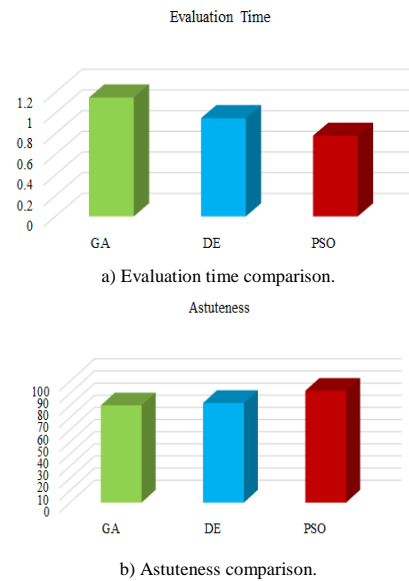
Figure 17. Comparison of performance parameters.

In addition the efficiency of the introduced methodology is assessed through the comparative analysis of classifiers based on the attained values of performance parameters, which is significantly portrayed in Figure 18 and Table 3 in an optimal manner.
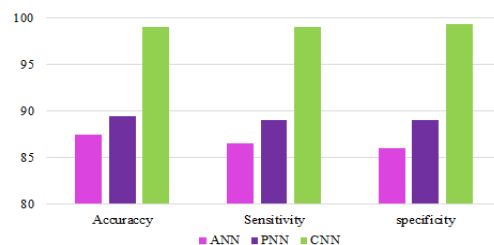
Figure 18. Performance efficiency evaluation.

Table 3. Performance analysis.

Parameters	Accuracy	Sensitivity	Specificity
ANN	87.4%	86.9%	87.2%
PNN	89.5%	89.1%	89.4%
CNN	99.2%	99%	99.1%

The accuracy of 99.2%, specificity of 99.1%, sensitivity of 99% attained as the outcomes of Convolutional Neural Network (CNN), which are comparatively optimal than the other classifiers like ANN and Probabilistic Neural Network (PNN). As all these parameters are highly efficient than others, the efficiency of the entire approach is remarkably high.

5. Conclusions

This paper presents an efficient technique for the astute detection of defected region of AAA and the pathological condition of ruptured region. It delivers fast quantitative analysis while performing the classification with grey neural network classifier. This

proposed technique enables the cardiac surgeon and radiologist to enhance the ability in diagnosis. In addition, it facilitates early detection of many diseases, which has helped in saving human life. Through this proposed technique, the targeted objective is attained with maximized accuracy of 99.2%, specificity of 99.1% and sensitivity of 99%. The comparative analysis of PSO with other approaches like GA and DE in terms of astuteness, precision, f-score and evaluation time is performed. When it is performed with optimization, Comparative analysis results in superior performance. By performing various experimental approaches, the performance evaluation is done and it generates an astute output. Thus, it is highly possible to implement this approach in other clinically used ultrasound systems.

References

[1] Apostolakis I., Karageorgos G., Nauleau P., Nandlall S., and Konofagou E., "Adaptive Pulse Wave Imaging: Automated Spatial Vessel Wall Inhomogeneity Detection in Phantoms and in-Vivo," *IEEE Transactions on Medical Imaging*, vol. 39, no. 1, pp. 259-269, 2020.

[2] Auricchio F., Ferrara A., Lanzarone E., Morganti S., and Totaro P., "A Regression Method Based on Noninvasive Clinical Data to Predict the Mechanical Behavior of Ascending Aorta Aneurysmal Tissue," *IEEE Transactions on Biomedical Engineering*, vol. 64, no. 11, pp. 2607-2617, 2017.

[3] Beevi Z. and Sathik M., "A Robust Segmentation Approach for Noisy Medical Images Using Fuzzy Clustering with Spatial Probability," *The International Arab Journal of Information Technology*, vol. 9, no. 1, pp. 74-83, 2019.

[4] Chen Z., Luo J., Lin K., Wu J., Zhu T., Xiang X., and Meng J., "An Energy-Efficient ECG Processor with Weak-Strong Hybrid Classifier for Arrhythmia Detection," *IEEE Transactions on Circuits and Systems II: Express Briefs*, vol. 65, no.7, pp. 948-952, 2018.

[5] Cheung G., Su W., Mao Y., and Lin C., "Robust Semisupervised Graph Classifier Learning with Negative Edge Weights," *IEEE Transactions on Signal and Information Processing over Networks*, vol. 4, no.10, pp. 712-726, 2018.

[6] Dawwd S., "GLCM Based Parallel Texture Segmentation using A Multicore Processor," *The International Arab Journal of Information Technology*, vol. 16, no. 1, pp. 8-16, 2019.

[7] Do H., Ijaz A., Gharahi H., Zambrano B., Choi J., Lee W., and Baek S., "Prediction of Abdominal Aortic Aneurysm Growth Using Dynamical Gaussian Process Implicit Surface," *IEEE Transactions on Biomedical Engineering*, vol. 66, no. 3, pp. 609-622, 2019.

[8] Guo Y., Jia X., and Paull D., "Effective Sequential Classifier Training for SVM-Based Multitemporal Remote Sensing Image Classification," *IEEE Transactions on Image Processing*, vol. 27, no. 6, pp. 3036-3048, 2018.

[9] He W., He Y., Li B., and Zhang C., "A Naive-Bayes-Based Fault Diagnosis Approach for Analog Circuit by Using Image-Oriented Feature Extraction and Selection Technique," *IEEE Access*, vol. 8, pp. 5065-5079, 2020.

[10] Hsieh S. and Chou Y., "A Faster CDNA Microarray Gene Expression Data Classifier for Diagnosing Diseases," *IEEE/ACM Transactions on Computational Biology and Bioinformatics*, vol. 13, no.1, pp. 43-54, 2016.

[11] Jan M. and Verma B., "A Novel Diversity Measure and Classifier Selection Approach for Generating Ensemble Classifiers," *IEEE Access*, vol. 7, no. 10, pp.156360-156373, 2019.

[12] Jin X., Gu Y., and Liu T., "Intrinsic Image Recovery From Remote Sensing Hyperspectral Images," *IEEE Transactions on Geoscience and Remote Sensing*, vol. 57, no. 1, pp. 224-238, 2019.

[13] Kurmi Y. and Chaurasia V., "Multifeature-Based Medical Image Segmentation," *IET Image Processing*, vol. 12, no. 8, pp. 1491-1498, 2018.

[14] Li M., Fang Z., and Lu S., "An Accurate Object Detector with Effective Feature Extraction by Intrinsic Prior Knowledge," *IEEE Access*, vol. 8, pp. 130607-130615, 2020.

[15] Li Q., Zheng B., Tu B., Wang J., and Zhou C., "Ensemble EMD-Based Spectral-Spatial Feature Extraction for Hyperspectral Image Classification," *IEEE Journal of Selected Topics in Applied Earth Observations and Remote Sensing*, vol. 13, pp. 5134-5148, 2020.

[16] Liu F., Bi F., Chen L., Shi H., and Liu W., "Feature-Area Optimization: A Novel SAR Image Registration Method," *IEEE Geoscience and Remote Sensing Letters*, vol. 13, no. 12, pp. 242-246, 2016.

[17] Mylonas S., Stavrakoudis D., Theocharis J., Zalidis G., and Gitas I., "A Local Search-Based GeneSIS algorithm for the Segmentation and Classification of Remote-Sensing Images," *IEEE Journal of Selected Topics in Applied Earth Observations and Remote Sensing*, vol. 9, no. 4, pp. 1470-1492, 2016.

[18] Peng B., Wang X., and Yang Y., "Region Based Exemplar References for Image Segmentation Evaluation", *IEEE Signal Processing Letters*, vol. 23, no. 4, pp. 459-462, 2016.

[19] Polanczyk A., Podgorski M., Polanczyk M., Piechota-Polanczyk A., Neumayer C., and Stefanczyk L., "A Novel Patient-Specific Human Cardiovascular System Phantom (HCSP) for Reconstructions of Pulsatile Blood

Hemodynamic Inside Abdominal Aortic Aneurysm," *IEEE Access*, vol. 6, no. 10, pp. 61896-61903, 2018.

[20] Pratama M., Pedrycz W., and Lughofer E., "Evolving Ensemble Fuzzy Classifier," *IEEE Transactions on Fuzzy Systems*, vol. 26, no.5, pp. 2552-2567, 2018.

[21] Qi F., Liang F., Liu M., Lv H., Wang P., Xue H., and Wang J., "Position-Information-Indexed Classifier for Improved Through-Wall Detection and Classification of Human Activities Using UWB Bio-Radar," *IEEE Antennas and Wireless Propagation Letters*, vol. 18, no. 3, pp. 437-441, 2019.

[22] Ren X., Wu Y., Wang L., Yan X., Zhang L., Cao Z., and Lin H., "Three-Dimensional Reconstruction of Abdominal Aortic Aneurysm Based on Compressive Sensing with Iterative Optimization and Its Application in 3D Printing," *IEEE Access*, vol. 7, no.11, pp. 170012-170018, 2019.

[23] Shen J., Cao X., Li Y., and Xu D., "Feature Adaptation and Augmentation for Cross-Scene Hyperspectral Image Classification," *IEEE Geoscience and Remote Sensing Letters*, vol. 15, no. 4, pp. 622-626, 2018.

[24] Toksöz M. and Ulusoy I., "Hyperspectral Image Classification via Basic Thresholding Classifier," *IEEE Transactions on Geoscience and Remote Sensing*, vol. 54, no. 7, pp. 4039-4051, 2016.

[25] Venkatesan A. and Parthiban L., "Medical Image Segmentation with Fuzzy C-Means and Kernelized Fuzzy C-Means Hybridized on PSO and QPSO," *The International Arab Journal of Information Technology*, vol.14, no. 1, pp. 53-59, 2017.

[26] Wei B., Zhang W., Xia X., Zhang Y., Yu F., and Zhu Z., "Efficient Feature Selection Algorithm Based on Particle Swarm Optimization with Learning Memory," *IEEE Access*, vol. 7, no.11, pp.166066-166078, 2019.

[27] Zhang L., Jiang X., Choi J., Lim C., Maiti T., and Baek S., "Patient-Specific Prediction of Abdominal Aortic Aneurysm Expansion Using Bayesian Calibration" *IEEE Journal of Biomedical and Health Informatics*, vol. 23, no.6, pp. 2537-2550, 2019.

Anandh Sam Chandra Bose is working as Associate Professor in the department of Biomedical Engineering, Saveetha Engineering College, Chennai. He has 20 years of teaching experience. His areas of interest are medical Image processing, Bio-signal processing and biomedical Instrumentation.

Vasuki Ramesh is working as Professor and Head in the department of Biomedical Engineering, Bharath Institute of Higher Education and Research, Chennai. She has 20+ years of teaching experience. Her areas of interest are Bioinformatics, Bio-signal processing and Image processing.

Appendix

Algorithm for particle swarm optimization

Input: fitness function, w, c_1, c_2, N_p

> *Initialize a random population and velocity within the bounds*
> *Evaluate the objective function value (t) of p*
> *Assign P_{best} as P and f_{pbest} as f*
> *Identify the solution with best fitness and assign the solution as g_{best} and fitness as f_{gbest}*

For t=1 to T
  For I =1 to N_p

> *Determine the velocity (v_i) of ith particle*
>
> *Determine the new position (x_i) of ith particle*
>
> *Bound X_i*
>
> *Evaluate the objective function value of ith particle*
>
> *Update the population by including x_i and f_i*
>
> *Update $p_{best,i}$ and f_{best}*
>
> *Update g_{best} and f_{gbest}*

  End

End